CLM-P670

UKAEA

Preprint

LASER TREATMENT OF GREY IRON

D. N. H. TRAFFORD
T. BELL
J. H. P. C. MEGAW
A. S. BRANSDEN

CULHAM LABORATORY
Abingdon Oxfordshire
1982

CLM-P 670

LASER TREATMENT OF GREY IRON

D.N.H. Trafford[1], T. Bell[2], J.H.P.C. Megaw
and A.S. Bransden

UKAEA Culham Laboratory, Abingdon, Oxon OX14 3DB, UK.

ABSTRACT

A 5kW industrial CO_2 laser has been used to investigate the hardening response of Grade 17 type grey iron. A number of different beam intensities were used, and treatment rates were chosen to produce a range of case depths with and without surface melting. The investigation concentrated on three aspects: case depths achieved, metallurgical structures observed, and wear performance of the hardened tracks.

[1]University of Liverpool, Dept. of Metallurgy
[2]University of Birmingham, Dept. of Metallurgy and Materials.

(Paper to be published in Proceedings of Metals Society Conference 'Heat Treatment 1981')

MARCH 1982
/SJT

INTRODUCTION

High power carbon dioxide lasers (considered here as those with output > 500W) are gaining increasing acceptance for the surface treatment of materials and a number of their production applications are now fairly well established[1-3]. The process ranks with other localised thermal treatments such as those produced by electron beams, and precision plasma and induction sources. It shares with these the advantages that component bulk heating is minimised, thereby increasing efficiency, reducing distortion and possibly eliminating the need for an external quenchant. Furthermore, 'hardened patterns' can be achieved and it is claimed[3] for example that the use of a laser-hardened spiral on a shaft running in a bearing results in one third of the wear experienced by a uniformly induction-hardened shaft. This is because in the former case the wear products and other debris can become safely embedded in the softer interspiral zone.

In drawing comparisons between the laser and other localised sources, it is not surprising to find that the situation is fairly complex. Some of the competing technical features are summarised in Table 1, but in choosing the optimum process for a specific application, detailed consideration needs to be given to inter-related factors such as capital cost, component geometry, process speed, metallurgy and distortion. It is worth noting that despite the relatively high capital costs of electron beams and lasers they are being introduced into production line surface hardening operations.

Table 1

Thermal Source	Principal Technical Features	
	Laser compared with named source.	Named source compared with laser.
Electron Beam	No vacuum required. Mirrors can deflect beam around corners. One laser can service several workstations.	Absorbing coating unnecessary. Simplified beam programming. High efficiency of beam power generation.
Induction	Long stand-off possible. Heat pattern more readily changed. Less sensitive to component section/ profile. Higher intensity possible. No electrodynamic forces to displace melt layers.	Absorbing coating unnecessary. Simple technology. Well suited to creation of deep cases.
Plasma	No electrode effects. Heat pattern more readily changed. Higher intensity possible.	Absorbing coating unnecessary. Very simple technology.

Comparison of the processes will obviously be simplified by the availability of performance data, and the objective of the present work was to carry out a detailed assessment of the response of a common engineering material (Grade 17 cast iron) to laser surface treatment. A number of different beam intensities were therefore used, and treatment rates were chosen to produce a range of case depths with and without surface melting. The investigation concentrated on three aspects: case depths achieved, metallurigcal structures observed, and wear performance of the hardened tracks.

Principles of Laser Processing

For the treatment of engineering components the laser can be regarded simply as a device for producing a finely controlled heating beam. The laser beam can rapidly raise the surface temperature of metal, and removal of the energy source results in self quenching by conduction of heat into the bulk, thereby producing a rapidly cooled surface layer. It is convenient to characterise the process in terms of the beam power density, I, and the interaction time, τ ($\tau = \ell/v$ where ℓ is the length of the heating pattern in the scan direction and v is the scanning speed). The depth of material raised above a given temperature is governed strongly by energy density $I\tau$, where low power densities and long dwell times will produce longer heating, holding and quenching times than those achieved using high power density and short dwell time. Thus is is possible with suitable steels and cast irons to produce in a controlled manner (a) surface hardened zones and (b) surface melted zones.

Surface hardening has been investigated in a previous paper[4] where the authors demonstrated the uniformity of treatment which can be achieved by a single pass of the laser. In those experiments a cast iron substrate was hardened to a depth of 0.25mm in a band approximately 14mm wide, using an absorbed power density (APD) of 1.6kW cm^{-2} at a coverage rate (C.R) of 140cm^2 min^{-1}. When significant surface coverage is required, successive passes can be laid down side by side or overlapped slightly and in order to minimise the formation of tempered regions between neighbouring passes, a sharp edged beam is employed. Figure 1 demonstrates the tempering effect at a depth of 0.1mm below the surface of a 2½% Ni-Cr-Mo steel produced by two converging laser passes. The width of each track was approximately 11.3mm and where the passes overlapped by 1mm (cross section No. 2), the tempered zone was also confined to a similar width. As the amount of overlap was increased the degree of tempering and the width of the heat affected zone became more pronounced.

Melting of the surface can be achieved by adjustment of the laser processing parameters, and this forms the basis of surface alloying, cladding and rapid solidification treatments. This last named treatment has successfully been employed with grey iron components used in the machine tool and textile industries[3,5]. The benefits of the treatment are thought to result from a re-cast zone with an ultrafine microstructure of exceptional hardness[4].

Equipment and Trials Procedure

The laser treatment was carried out at Culham Laboratory on a laser system which incorporates a 5kW CO_2 laser model CL5 and three workstations. The operating principles of the laser were outlined previously[4], and Figure 2 shows workstation Number 1 which is mainly used for surface treatment work. Surface hardening normally requires extended, uniform heating patterns (typical dimension of order 10mm) and these were achieved using a vibrating mirror technique. The incident laser beam, of outer diameter approximately 50mm, is focused by a mirror (f/100) on to the workpiece, over a path which includes two plane mirrors, vibrating on perpendicular axes at frequencies ~ 300Hz. Thus the focused spot is 'rastered' at high speed to create a heating pattern of readily variable size. The simple harmonic nature of the mirror vibration results in enhancement of the power density at the edges of the pattern, and an absorbing mask may be employed to alleviate the effect. In this development work, where uniform intensities were sought and typically $\pm$ 15% obtained, masks were employed although this caused transmission losses up to 50%. It should be noted that for component treatment the required intensity patterns are not necessarily flat-topped, and can frequently be achieved without masks or with alternative beam shaping techniques having high transmission. For most of the studies of the scaling of case depth with power density and interaction time, the beam spot width was 7mm and lengths in the travel directon were 3, 6 or 12mm. The specimens for wear testing were produced by a beam spot width of 10mm.

The sample material used was a Grade 17 Meehanite G.C., the composition range of which is given in Table 2 [6]. Described as an easily machinable iron with a fine, close grain, this material is commonly used in the manufacture of machine tool beds, cams, piston rings, pistons, cylinders, etc[7]. Structurally, the material consists of medium size flake graphite in a matrix of fine lamellar pearlite without any phosphide eutectic but with a random distribution of approximately 2% free ferrite. The material is well suited to laser treatment since the fine pearlitic structure ensures complete

austenitization to appreciable depths during the short heating cycle although the free ferrite remains.

Test pieces measuring approximately 150 x 50 x 10mm were machined from cast bar stock, and two surface finishes were investigated: ground (0.4μm (Ra) finish) and milled (1.5μm (Ra) finish). Figure 3 shows a typical specimen after treatment. For efficient beam coupling in surface hardening, an absorbing coating is required, and in the present work colloidal graphite was applied as a spray at a coverage of approximately 0.7mg cm^{-2}. The effective absorptivity was not monitored in this work, but it is known[8] that below onset of surface melting, an effective absorptivity of approximately 80% is observed for a range of coatings. Therefore, throughout the paper it is assumed that absorbed power density is 80% of incident. It is however known that with onset of melting, absorptivity falls because of destruction of the coating. It should be noted that at very slow scan speeds and with greater melting, the absorption of these low intensities will rise again as surface disruption leads to beam-trapping effects; with the high intensities ($> 10^6$W cm^{-2}) used in laser welding, very efficient beam trapping is routinely achieved.

Results and Discussion

A. Case Depths

The conditions employed to produce a range of case depths are shown in Table 3. After treatment, the samples were transversely sectioned, polished, etched and the depth of the heat affected zone (HAZ, defined as the light-etching structure) at the track centre line was measured. Microhardness scans showed that the edge of the HAZ coincided with the start of increase of hardness above base value. It is seen from Table 3 that, for given process conditions the depths of HAZ obtained for ground and milled finishes were not significantly different. Figure 4 shows a macrograph of the sample cross section produced with absorbed power density 4.8 x 10^3W cm^{-2} and an interaction time of 0.15s, where it is seen that uniformity of case depth is good. The use of high power densities and short interaction times favour the creation of HAZ cross sections which mirror the incident intensity distribution i.e. the heat flow can be regarded as predominantly one dimensional normal to the material surface. Low power densities and long interaction times result in enhancement of depth at the track centre line.

Figure 5 shows the HAZ depths of Tables 3 plotted against reciprocal of

beam interaction time (which is proportional to the beam scan speed in our approximation). Also shown by solid lines are the predictions of a one dimensional heat flow model[8] for the depth of material raised above 800°C. This temperature, slightly above the eutectoid value, was chosen to compensate for the short holding time of the process. The calculation used values of thermal conductivity $K = 0.42\ Wcm^{-1}\ {}^{o}C^{-1}$, thermal diffusivity $k = 7.2 \times 10^{-2}\ cm^2\ s^{-1}$, melting point 1140°C. The predictions are shown for absorbed power densities of 1, 3 and $6 \times 10^3 W\ cm^{-2}$ and the onset of melting is shown by a broken line. The agreement between theory and experiment is fair, bearing in mind that (i) the absorption is not constant but, for example, decreases as surface melting is approached, and (ii) particularly for low power densities and long interaction times (left-hand side of the figure) the assumption of one-dimensional heat flow is poor. The figure may also be used to indicate the higher process efficiency associated with high power density and short interaction time: to achieve a fixed case depth of 0.4mm, the absorbed energy density required (inversely proportional to efficiency) at 1.2, 2.4 and $4.8kW\ cm^{-2}$ respectively is approximately 4×10^3, 1.4×10^3, $1 \times 10^3 J\ cm^{-2}$. Physically, this is due of course to the reduction of bulk heating at high power density.

Figure 6 shows microhardness profiles as a function of depth and reciprocal of interaction time for the three absorbed power densities. The profiles show uniformity of case hardness except for shallow cases or when there is surface melting. With the approach of melting, the hardness level at the surface first falls and then rises significantly. The reasons for this are discussed below.

B. Metallurgical Characteristics

Besides providing an analysis of the various microstructures which can be produced by laser treatment, this section considers process problems and solutions associated with surface melting cast iron.

i. Surface Topography

Figures 7a to 7c show typical track topographies corresponding to transformation hardening, incipient melting and complete surface melting respectively. Figure 7b shows that incipient melting resulted in the production of isolated globules which formed as the result of surface tension effects. Increasing interaction times

produced a progressive increase in both the size and number of globules until eventually they joined together to create a continuous external melt layer (Fig. 7c). Examination of the tracks on samples which underwent surface melting to an appreciable depth (150μm) revealed a relatively smooth surface, although when viewed in cross section surface undulations were apparent. Cracks were also a feature of surface melted layers and their presence is discussed in more detail in a later section.

ii. Metallographic Examination

Figure 8a is a transverse cross section through a sample which has been surface hardened without melting. Figure 8b shows the microstructure at the case/core interface in more detail. The material in this zone has been heated to temperatures below the fully austenitizing temperature and consequently the structure and properties of this region are intermediate between those of case and core. Demarcation in structure between core and case is typically quite sharp and a similar sharp demarcation is usually observed when hardening by induction techniques[9]. Hardness measurements performed using a Leitz miniload microhardness tester with a load of 300g showed the case to be in the martensitic condition with a hardness of $850HV_{0.3}$ (Fig. 8c), which is virtually the maximum attainable hardness for this material. Hardness measurements also revealed slight overtempering of the core material in the boundary in zones up to 200μm wide, particularly on samples which were treated for the longest treatment times at the lower power density.

Figure 9a is a cross section through a hardened case with surface melting, which shows the three distinct regions in the case. First, the outer melt region, which had an extremely fine filamentary ledeburitic structure can be seen in more detail in Figure 9b. It is evident that the graphite flakes had completely dissolved in the molten ferrous material during treatment and rapid self quenching had suppressed the reformation of grey iron in favour of the formation of white iron. Second, in the intermediate region at the bottom of the melt layer only partial dissolution has occurred and the graphite flakes, although thinned, had been retained. Figure 9c shows this layer was comprised of a mixture of retained austenite and coarse martensite plates. Also present in this figure is a

graphite flake surrounded by ledeburite protruding from the outer melt layer. This combination was a common feature at the irregular melt interface and indicated that as the melt layer encroached into the substrate it was the material in the vicinity of the graphite flakes which melted initially. This occurs, of course, because carbon enrichment adjacent to graphite flakes locally lowers the melting point of the ferrous material. Finally, the inner region of the case consisted of fine unresolvable martensite.

Figure 10a shows a hardness profile across a case which exhibited surface melting. Measurements gave typical values in the range $600/700HV_{0.3}$ for the intermediate zone and $950HV_{0.3}$ for the material in the melt layer. The cementite content directly influenced this latter value, but the exceptional hardness was not only a reflection of a distribution of fine cementite platelets in the melt layer but also the result of primary ledeburitic austenite transforming to martensite on cooling[5]. On samples exhibiting incipient melt phenomena attempts were made to measure the hardness of the globules in cross section, but the globules were too shallow. Measurements taken on the crown of globules, however, using a 100g. load gave a value of $900HV_{0.1}$. Figure 10b shows incipient melting always manifested its presence by the formation of a softer skin (typical hardness $700/800HV_{0.3}$) especially on samples which were processed for the longest treatment times at the lower power density.

iii. Sub-Zero Treatment of Laser Melted Layers

The zone of retained austenite associated with surface melting is undesirable since besides adversely influencing the mechanical properties of the hardened layer, it has the potential for strain induced transformation. Austenite is retained after treatment because the solid material just beyond the limit of melt penetration becomes enriched in carbon due to enhanced carbon diffusion from graphite flakes and from molten surface metal. The ferrous material in the zone therefore acquires a carbon content in excess of the normal eutectoid value of 0.8%, together with an increased tendency to retain austenite.

Figure 11 shows the effect on case hardness of a 10 minute sub-zero treatment in liquid nitrogen. A slight increase in the hardness of

the inner martensite layer is produced and the level of hardness of the material in the intermediate layer is raised to that of the inner layer.

iv. The Problem of Cracking Associated with Surface Melting

In this work it was found that treatment conditions which avoided surface melting produced tracks completely free of cracks; however, when surface melting was present, the tracks normally exhibited cracking (Figure 7c). The cracks which develop are usually isolated and extend through the melt zone appearing to stop in the intermediate zone (Fig. 12). Possible causes of cracking are:

a. The treatment produces a surface layer of white iron which undergoes a solidification contraction of approximately 4%.

b. The presence of an unacceptably high population of inclusions[10].

c. The increase in volume associated with the formation of an inner layer of martensite after the brittle outer white iron has solidified, which may set up residual tensile stresses.

The problem of cracking has previously been observed in the welding and TIG hardening[11] of grey iron components and has been successfully overcome by preheating the material to 400°C. Essentially the treatment is a residual heat tempering process which besides limiting the incidence of cracking also reduces the amount of retained austenite.

C. Wear Testing

A conventional reciprocating pad-on-plate technique was used to evaluate wear resistance of the various microstructures produced by laser treatment. The test blocks were clamped to the wear machine and were oscillated at a frequency of 2.5Hz beneath a stationary 8mm diameter SiC wear pad under an applied load of 5.0kg. Tests were performed in the unlubricated condition to produce wear scars measuring approximately 25 x 8mm on the surface of the tracks. The mass of the assembly was sufficient to prevent bulk heating of the test-piece during testing.

After the completion of each wear test, which ranged from 2-7 days depending upon the microstructure being investigated, stylus profiling of the wear scars was performed with a Taylor-Hobson Talysurf in order to

obtain a measure of the volume of material removed. A wear rate was then determined and expressed as a volume loss per distance travelled per kilogram load.

Wear tests were performed on samples having the three different microstructures described and these results were compared with those of the base material in the as-cast condition. The wear rates for each of the representative microstructures are ranked in order of increasing abrasion resistance in Figure 13. The superior wear resistance of surface melted microstructures can be seen. Prior to testing it was necessary to lightly grind samples in conditions B and D to re-establish a planar surface.

Figure 14 shows the topographical appearance of the wear scars as revealed by scanning electron microscopy. After 2 days testing the untreated material exhibited considerable wear, including gouging and breaking up of the surface layer. After 7 days testing, similar gouging was also present on the surface of sample in condition B, but the microstructures corresponding to conditions C and D showed little evidence of wear.

Conclusions

This work on grey iron has demonstrated the high degree of control that can be exercised in laser hardening to produce a range of case depths and microstructures. A one-dimensional heat flow model provided an adequate prediction of the experimental results. It should be noted that full modelling of the process would be very difficult due to the metallurigcal transformation kinetics involved and the complex dependence of beam coupling on the process conditions. However, the approach described has been found to facilitate rapid process optimizaton in component treatments.

Cases produced without surface melting attained a uniform hardness which was virtually the maximum for this material, but when surface melting was achieved there was a further significant increase in case hardness. This increase was reflected in the superior abrasion resistance of surface melted microstructures.

Although there is yet scope for further research and development, the present work has nevertheless shown that laser treated cast iron clearly has a future

as an engineering material.

Acknowledgements

The authors are indebted to Mr. M. Farrow of the National Tribology Centre, Risley for the provision of wear testing facilities and to Mr. K.T. Stevens of the National Tribology Centre for valuable technical assistance in the preparation of wear data. The interest in this work of Dr. I.J. Spalding and members of the Culham Laser Applications Group is greatly acknowledged.

References

1. J.E. Miller, J.A. Wineman; Metal Progress, 1977 111, May p38.
2. Anonymous; Heat Treating, 1978, July, p22.
3. J. Taylor; Metalworking Production, 1979, Sept. p138.
4. D.N.H. Trafford, T. Bell, J.H.P.C. Megaw, A.S. Bransden; Proc. of Heat Treatment '79, Metals Society/American Society for Metals, Birmingham, U.K. May 1979, p32.
5. A.N. Kokora, A.A. Zhukov, L.Z. Ephstein; Fiz. Khim. Obrabot. Mater., 1977, 11 No. 3, p24.
6. B. Mills; Richards Foundries Ltd., Leicester, Private communication.
7. Meehanite Specification Handbook, Int. Meehanite Metal Co. Ltd., Surrey.
8. J.H.P.C. Megaw, A.S. Kaye; Proc. of 4th European Electro-Optics Conf., Society of Photo-Optical Instrumentation Engineers, Utrecht, Netherlands, Oct. 1978, p24.
9. 'The Surface Hardening of Cast Iron', published by the British S.G. Iron Production Association, London.
10. W. Gowan; A.E.G. Elotherm (GB) Ltd., Dukinfield, Private Communications.
11. F.H. Reinke, Heat Treatment of Metals, 1981, 1, p17.

Table 2 - Composition of Grade 17 Meehanitic G.C.

Element	Wt%
C	2.9 - 3.2
Si	1.7 - 2.1
Mn	0.5 - 0.8
P	0.1 Max
S	0.06 - 0.11

Table 3 - Process Parameters

Beam Spot Size Length, ℓ x width mm x mm	Absorbed Power Density* $kW\ cm^{-2}$	Beam Interaction Time $\tau = \frac{\ell}{v}$ s	HAZ Depth mm
15 x 10	1.1	7.9 6.3 5.2 4.0	1.4** 1.0** 0.85** 0.65**
12 x 7	1.2	6.0 4.0 3.16 3.16 2.4 2.0 2.0	0.75 0.3 0.3 0.4** 0.15 0.1** 0.05
7 x 10	2.3	3.3 2.9 2.5 2.1	1.62** 1.31** 1.25** 1.08**
6 x 7	2.4	1.67 1.0 1.0 0.75 0.6 0.5 0.38 0.38 0.3	1.0 0.7 0.75** 0.55 0.45 0.27 0.15 0.13** 0.05
3 x 7	4.8	0.79 0.5 0.5 0.38 0.25 0.19 0.15 0.15 0.15 0.125 0.107 0.09	1.0 0.8 0.8** 0.7 0.45 0.34 0.18 0.3 0.33** 0.15 0.15 0.08

* Assuming 80% absorption
** Ground finish (others milled)

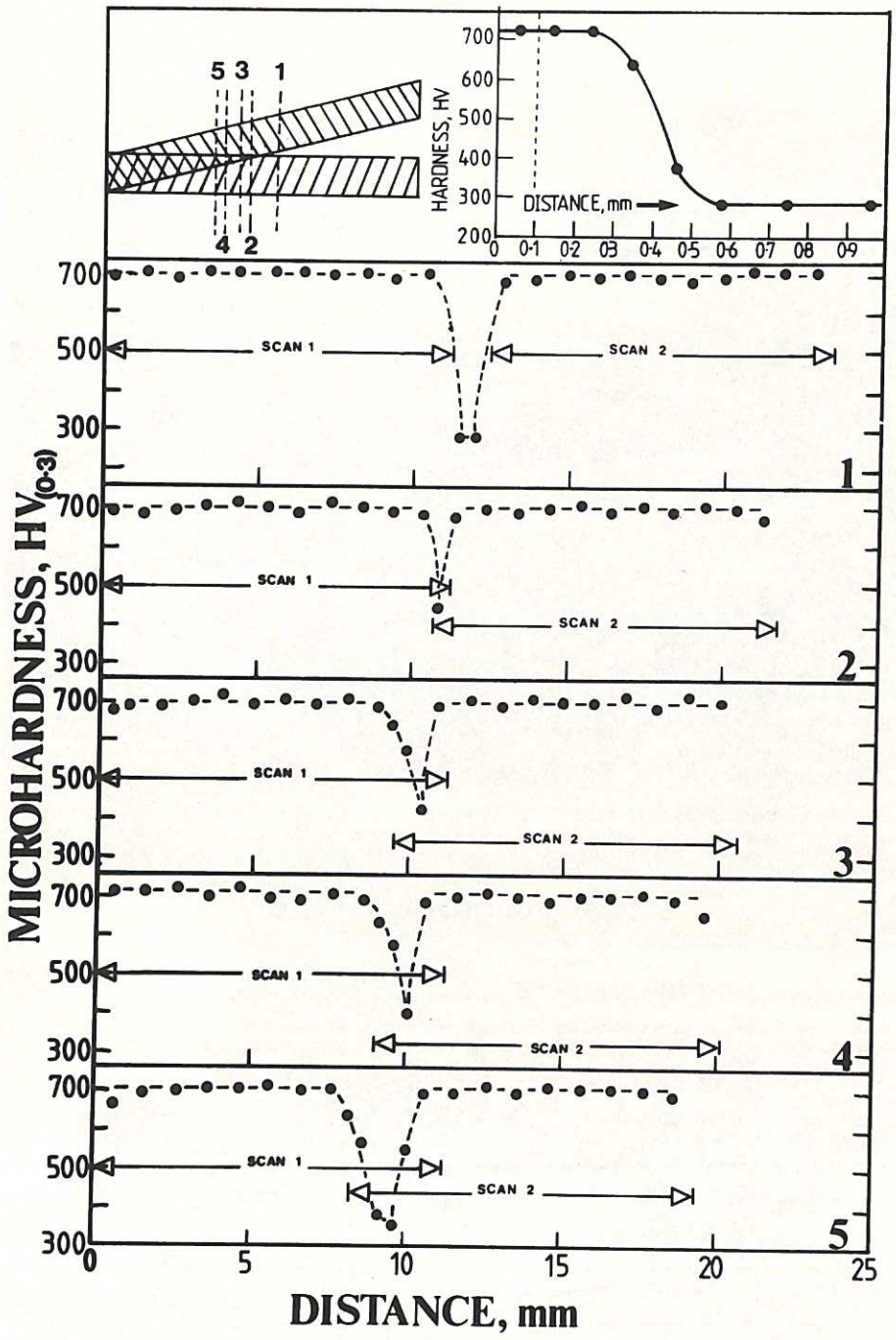

Fig.1 The tempering effect produced at a depth of 0.1 mm below the surface of 2½% Ni-Cr-Mo steel by two converging and overlapping scans. A.P.D. 1.0kW cm^{-2}, C.R. 27 cm^2 min^{-1}.

Fig.2 Workstation showing optical arrangement for heat treatment operations.

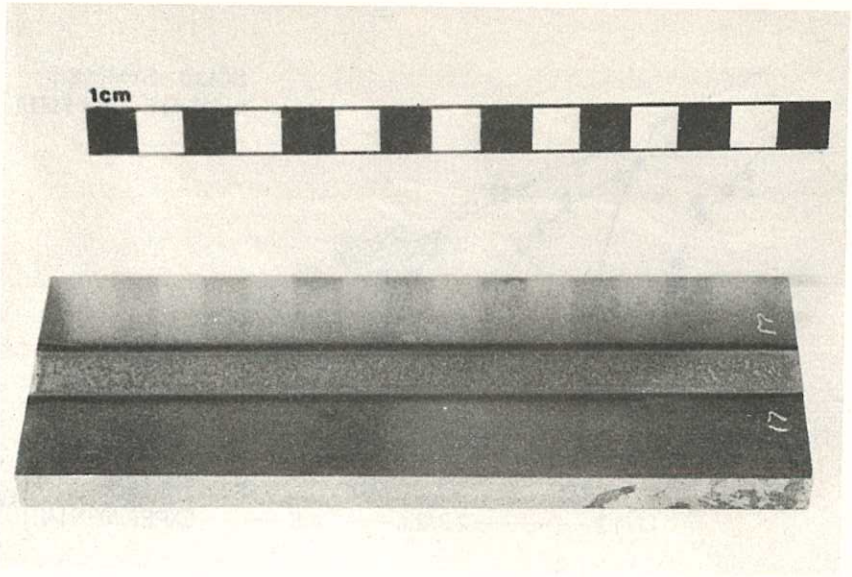

Fig.3 Testblock showing a hardened track produced by laser treatment.

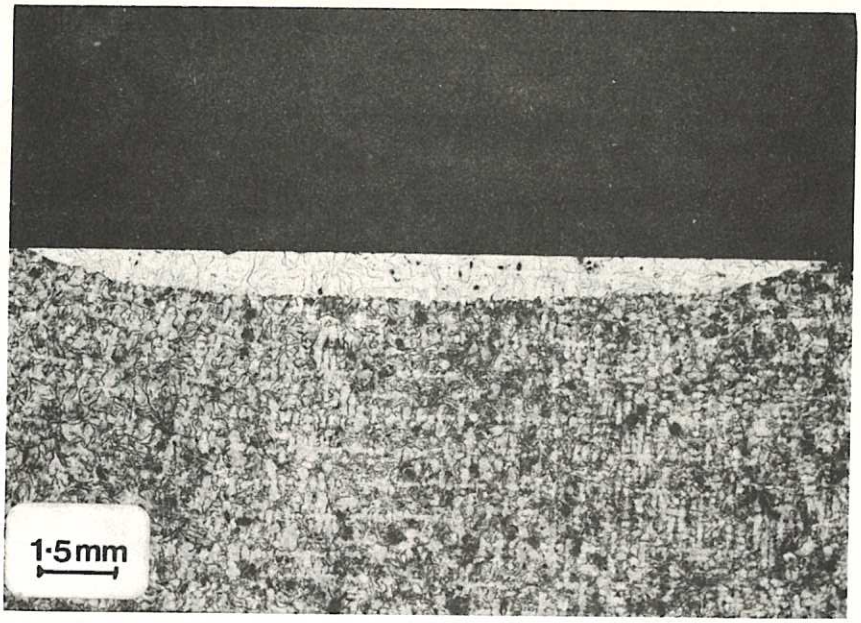

Fig.4 Micrograph showing macrosection of a hardened case;
A.P.D. 4.8kW cm^{-2}, C.R. 84cm^2 min^{-1}.

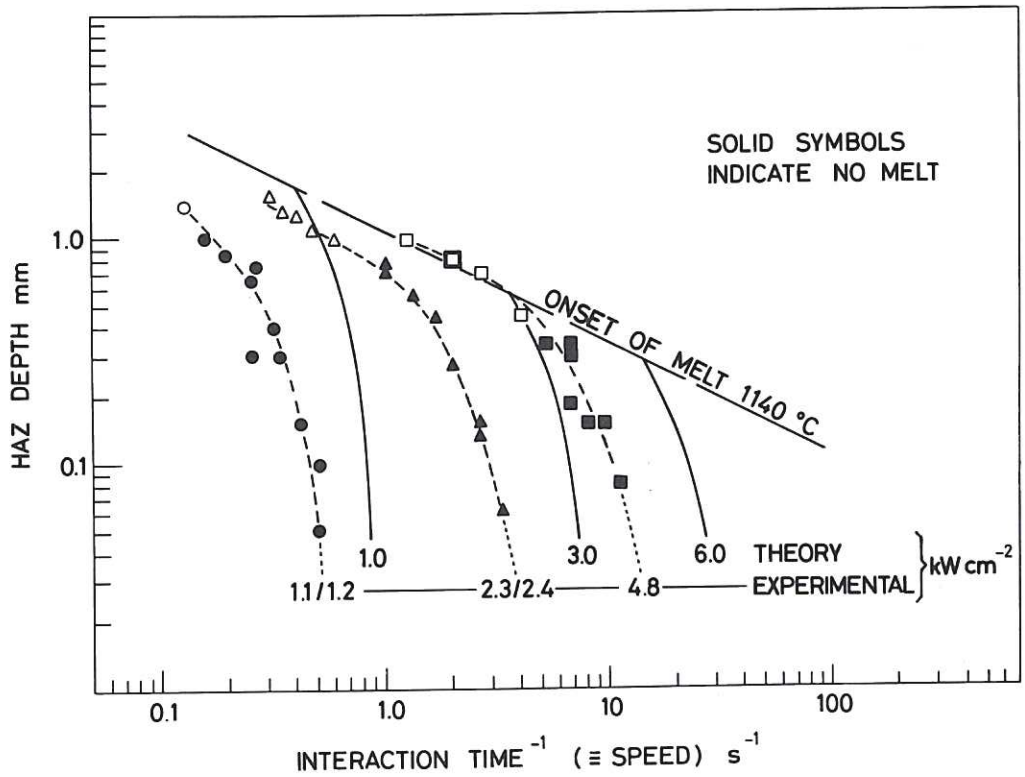

Fig.5 Theoretical and measured hardening depth as a function of $\frac{1}{\tau}$ (reciprocal of interaction time) for selected power densities.

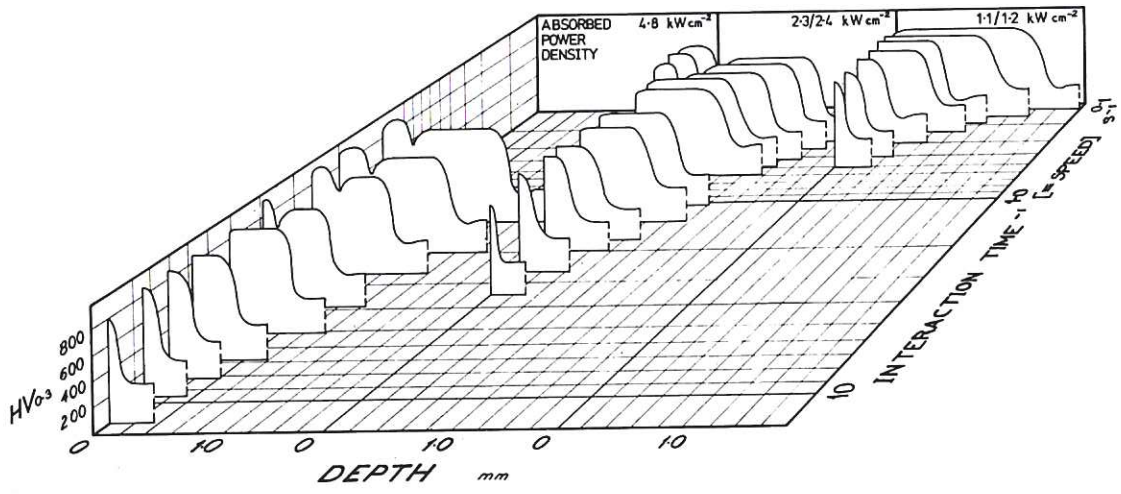

Fig.6 Hardness versus depth versus $\frac{1}{\tau}$ for the three power densities.

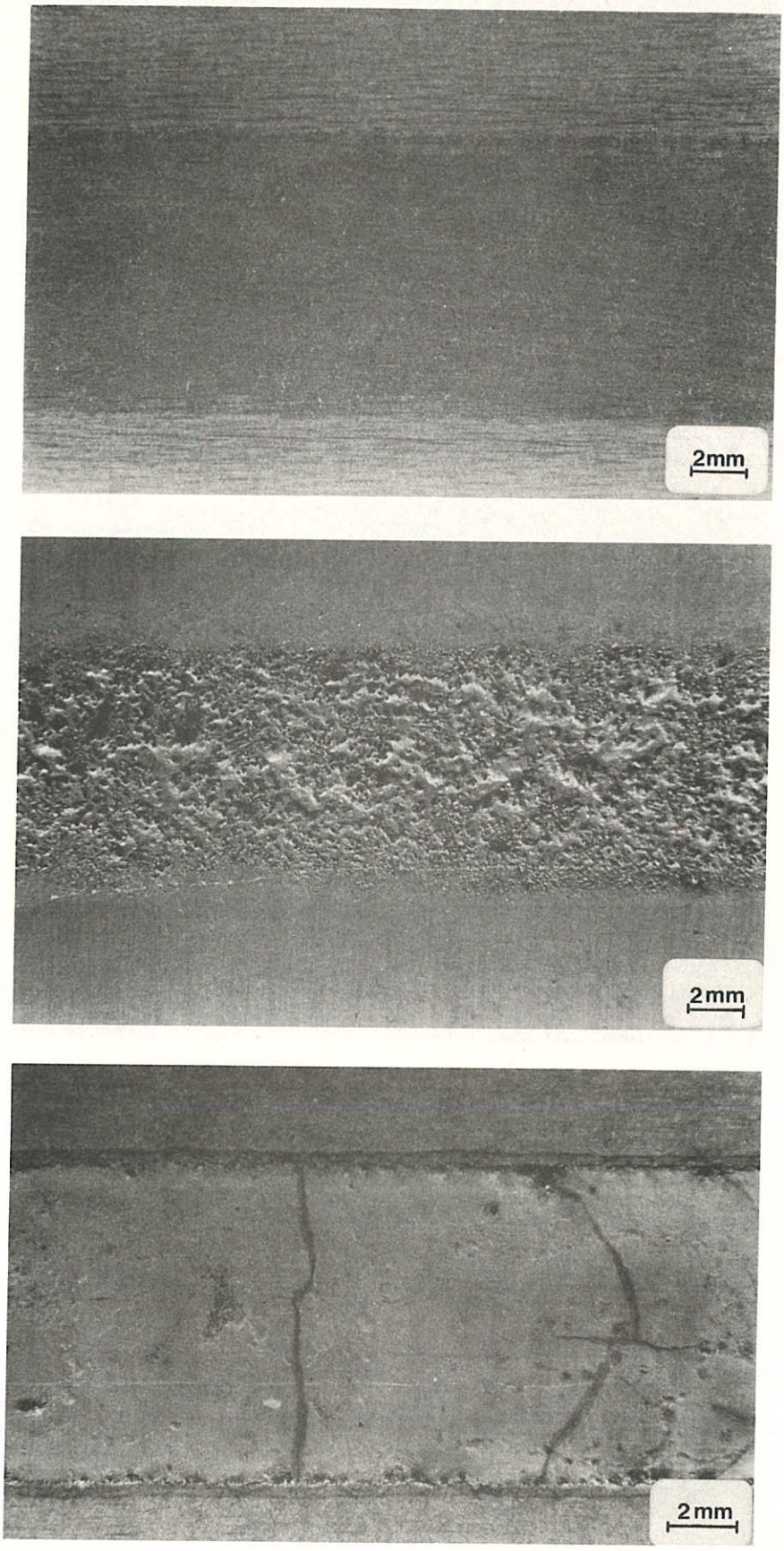

Fig.7 Typical topographical morphologies of: (a) hardened track without surface melting (b) partially melted track (c) fully melted track.

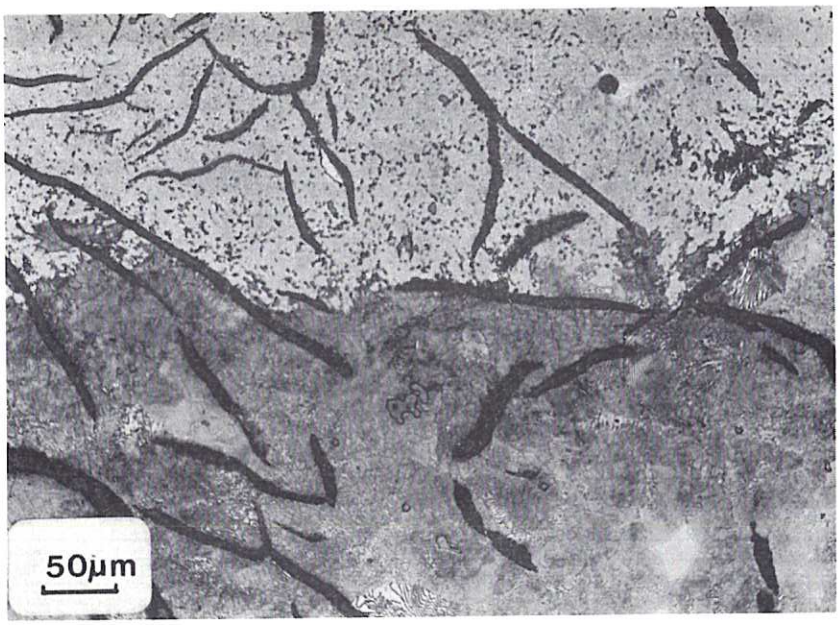

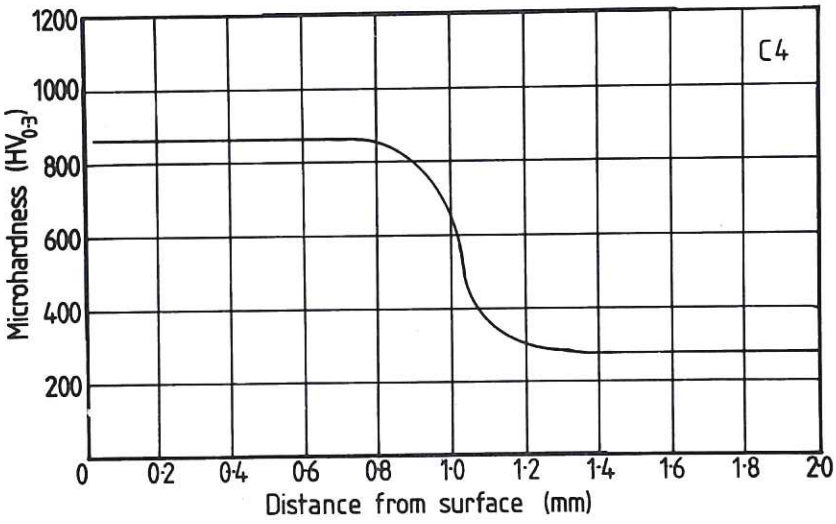

Fig.8 (a) Micrograph showing a laser hardened case without surface melting; A.P.D. 1.1kW cm^{-2}, C.R. 14$cm^2 min^{-1}$. Etched in nital.
(b) Micrograph showing the case/core interface in detail.
(c) Microhardness profile.

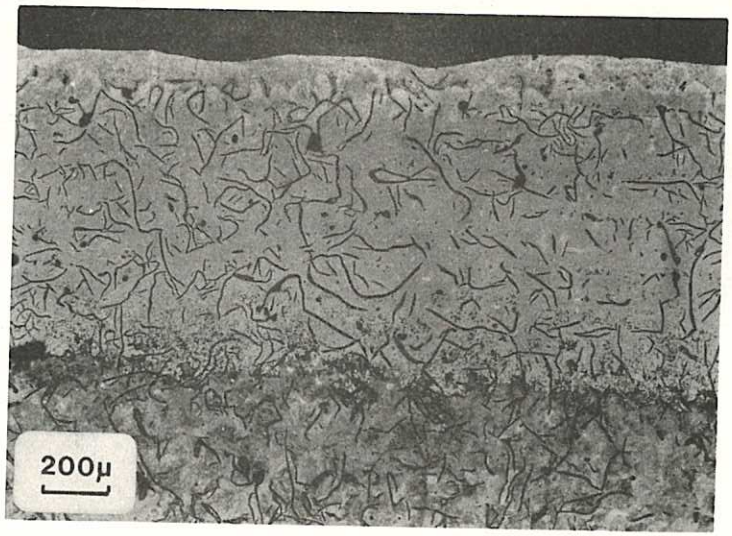

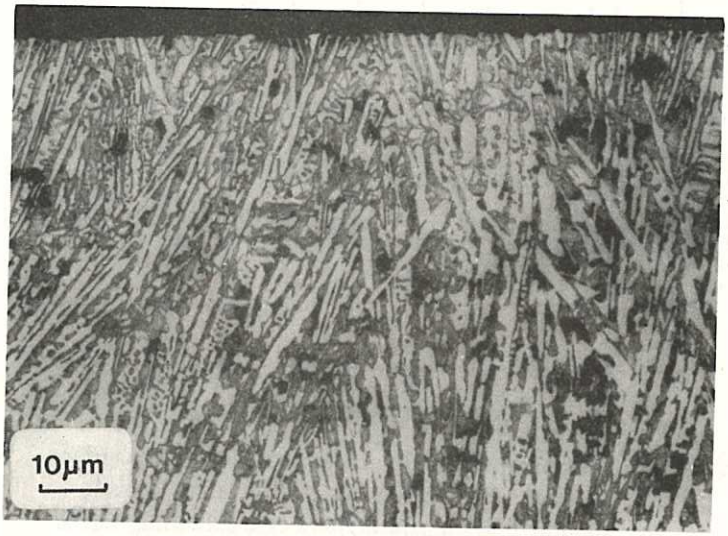

Fig.9 (a) Micrograph showing a laser hardened case with surface melting; A.P.D. 2.4 kW cm^{-2}, C.R. 15 cm^2 min^{-1}. Etched in nital.
(b) Micrograph showing the outer melt layer in detail.
(c) Micrograph showing the melt boundary in detail.

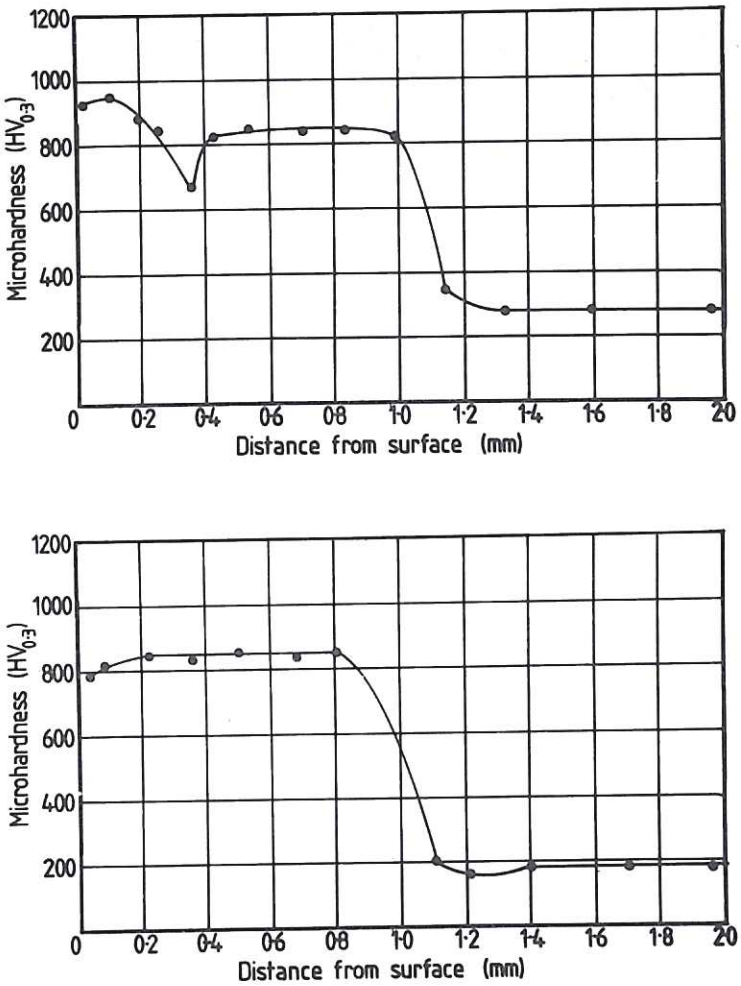

Fig.10 (a) Microhardness profile across a case exhibiting surface melting; A.P.D. 4.8kW cm^{-2}, C.R. 16 cm^2 min^{-1}.

(b) Microhardness profile across a case exhibiting partial surface melting; A.P.D. 2.4kW cm^{-2}, C.R. 15 cm^2 min^{-1}.

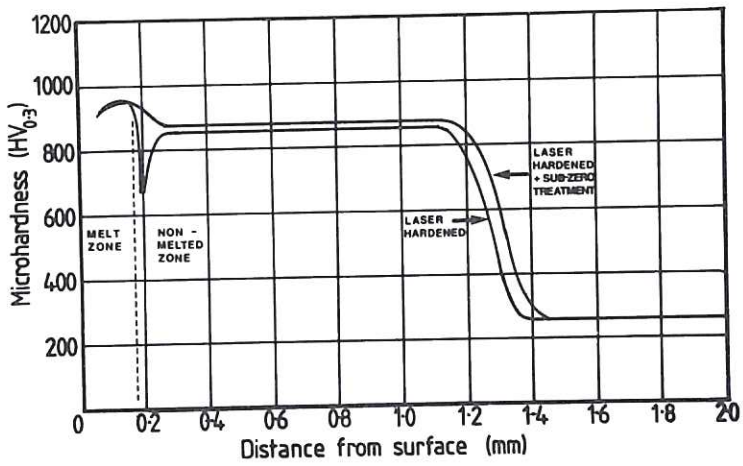

Fig.11 Microhardness profiles across surface melted track before and after sub-zero treatment.

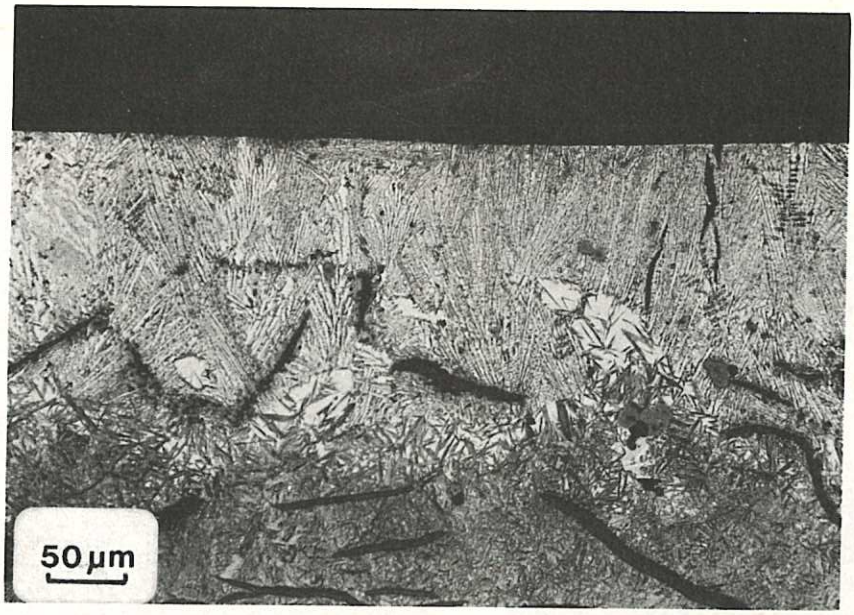

Fig.12 Micrograph showing microcracks in a surface melted case; A.P.D. 2.4kW cm^{-2}, C.R. 15 cm^2 min^{-1}. Etched in nital.

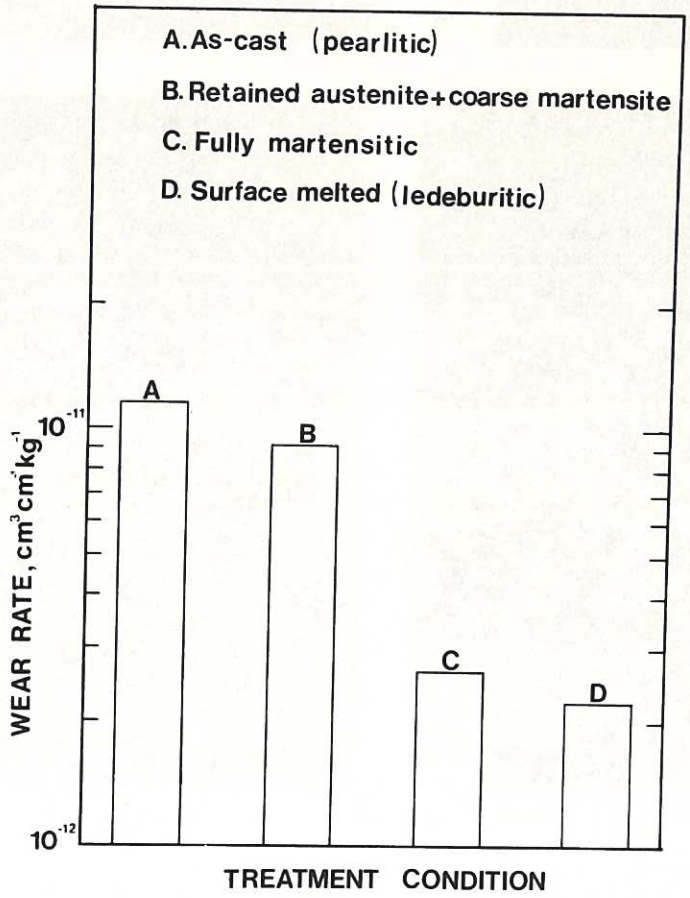

Fig.13 Comparison of the abrasive wear rates of various microstructures resulting from laser treatment.

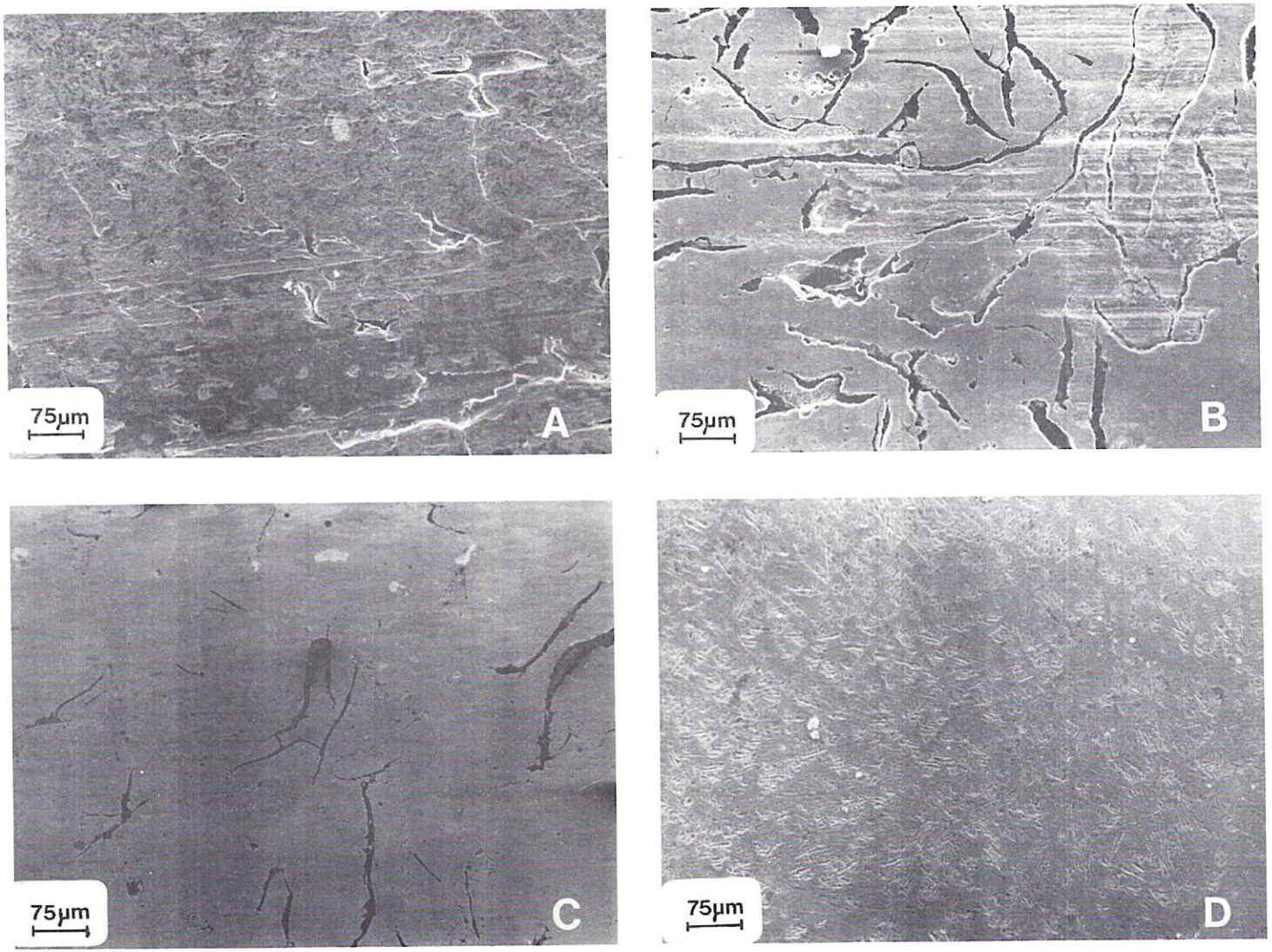

Fig.14 Scanning electron micrographs showing wear surfaces: (a) as cast, after 2 days testing, (b) retained austenite plus coarse martensite, after 7 days testing, (c) martensite, after 7 days testing, (d) ledeburite, after 7 days testing.